# A Periodic Density Functional Theory Study of Cumene Formation Catalyzed by H-Mordenite†

**X. Rozanska,* L. A. M. M. Barbosa, and R. A. van Santen**

*Schuit Institute of Catalysis, Laboratory of Inorganic Chemistry and Catalysis, Technical University of Eindhoven, P.O. Box 513, NL-5600 MB Eindhoven, The Netherlands*

*Received: February 20, 2004; In Final Form: April 20, 2004*

A periodic density functional theory study of the alkylation of benzene with propene in proton-exchanged mordenite has been achieved. The two different reaction routes that are usually proposed for this reaction, namely the direct and the step-by-step reaction pathways, have been investigated. The explicit consideration of the zeolite catalyst framework allows a better level of description of the interactions between the catalyst framework and the reaction than what is obtained with the cluster approach method. The direct reaction route is found to be the preferred one. It is observed that the cluster approach method, which does not describe the zeolite framework, is unable to qualitatively described the trend in activation energies. This is owing to the greater stabilization of larger transition state by the mordenite zeolite framework compared with smaller ones.

## Introduction

Zeolites are aluminosilicate crystals.[1] They have well-defined microporous structures based on the assembly of tetrahedral $SiO_4$ units that connect to each other by their oxygen atoms. Zeolites are chemically active when substitutions of silicon with aluminum occur. To balance the excess of charges, cations are present. Further chemical treatments of these zeolites are necessary to turn the material to a catalyst. Cation zeolites can be converted to protonic zeolites; then, one obtains solid acid catalyst.[1,2] Other chemical treatments exist, and zeolites can be acidic, basic, and/or redox catalysts.[3] Moreover, zeolites can be employed as general catalyst support via impregnation/deposition processes.[2b,4] Finally, combinations of catalytic sites are possible.[4]

The zeolite framework, as catalyst or catalyst support, is interesting for several reasons. First, zeolites show good thermal and mechanical stability.[4] This avoids too frequent renewal of catalyst load in the reactor. Second, zeolites have well-defined microporous networks. This induces shape-selective effects in zeolite catalysis.[5] Let us give more details on this last point.

The shape-selectivity of zeolitic catalysts has different origins, which can be present independently or in a combination to each other.[6] One parameter leading to selectivity in zeolite catalysis is size-selection.[5,6] Molecules that are too large to enter within the zeolitic micropore will not react. Products that are too large to fit within the micropores will not be formed (or will not leave the micropore network). However, size-selection can be obtained in many reactions taking place in the interior part of the zeolite. The most illustrative example of size-selectivity in zeolite catalysis is the selection between competitive mono- and bimolecular reaction pathways.[5,7,8]

Another way to get selectivity in a zeolite-catalyzed reaction is to exploit the match between the shape of molecule and that of the zeolite micropore. As a function of the size and shape of the molecules and geometry of the zeolite micropores, diffusivity constants of molecules differ.[6,9−11] This leads to products with a higher diffusivity constant representing a larger fraction in the products.[5] Product and reactant adsorption have been demonstrated to be essential parameters that follow the enthalpy−entropy compensation rule.[9] The product that will be formed or react with highest rate is the one that shows the best fit (enthalpically and entropically) within the zeolite micropores.[6,9,10]

The other important selectivity parameter relevant to zeolite catalysis is the shape and size of the transition state structure of an elementary reaction step with respect to the zeolite micropore geometry. To be converted into a product, a reactant has to evolve through intermediate and transition structural states. During a reaction, chemical bonds are broken and/or formed. More than 100 different reported structures of zeolites exist.[12] Hence, there is ample opportunity for optimization of structural choices when transition state structures are known. The main information on transition state selectivity derives from quantum chemical methods, as these methods constitute the only tool to allow an evaluation of transition state structures.

The recent progress both in quantum chemical methods and computer power allows now to investigate transition states in great detail. It is possible to analyze the interactions of the reactants, products, and their intermediates with the zeolitic catalytic site, as well as the structure and energy of corresponding transition states. Physisorption of reactants and products to the catalytic site is also important.[6,13] Molecular mechanical methods now have become quite important, since van der Waals interaction parameters can be incorporated.

Quantum chemical methods are very useful in the study of reactant and product adsorption to the catalytic site, as it is possible to compute spectroscopic properties such as the frequencies of vibration of the system.[6,14] This allows direct comparison of computed data with experimental infrared spectra.[15] Other electronic properties of the system can also be computed and compared to experimental data.[16] Moreover, not

† Part of the special issue "Michel Boudart Festschrift".

* Corresponding author: E-mail: tgakxr@chem.tue.nl. Present address: Institut fuer Chemie, Brook-Taylor-Str. 2, D-12489 Berlin, Humboldt-Universitaet zu Berlin, Unter den Linden 6, D-10099 Berlin, Germany.

10.1021/jp049227x CCC: $30.25 
Published on Web 05/27/2004

only stable intermediates but also transition states can be checked. Energy and frequency of vibrations of these different states can be computed. Employing transition state theory, it is then possible to estimate the rate constant of different reactions.[15,17]

In this report, we will present a periodic density functional theory study of cumene formation catalyzed by proton-exchanged mordenite. We have selected this reaction because it is an important industrial process.[4,18] Cumene is an intermediate in the production of phenol.[18,19] Mordenite zeolite is commercially employed to convert benzene and propene into cumene. Therefore, we chose this zeolite as the structure of choice in calculations. There are still extensive debates on the details of the reaction mechanism in the synthesis of cumene. The reaction has been suggested to occur via two possible reaction pathways.[18,19] The first reaction pathway is initiated by the chemisorption of propene to the zeolite wall. Consecutively, alkylation of benzene with isopropoxide takes place. The second reaction pathway happens in an associative way: in a concerted motion, propene is protonated and alkylates benzene directly. The first reaction pathway is sometimes described as consecutive or step-by-step reaction pathway, whereas the second is referred as associative or direct reaction pathway. So far, the alkylation of benzene with propene leading to the formation of cumene has never been investigated with a model including the entire structure of the zeolite catalyst, whereas it has been demonstrated to have a deep impact on reaction mechanisms.[7,8,20−23] The periodic density functional theory method allows to explicitly consider the zeolite framework and its effect on reaction.

## Methods

The periodic density functional theory calculations are performed employing the Vienna ab initio simulation package (VASP).[24−27] The total energy is calculated solving the Kohn−Sham equations using the local exchange-correlation functional proposed by Perdew and Zunger.[28] The results are corrected for nonlocality in the generalized gradient approximation with the Perdew−Wang functional (PW91).[29] VASP uses plane waves and ultrasoft pseudopotentials.[30] A 300 eV energy cutoff and a Brillouin zone sampling restricted to the Γ point were selected in our calculations. The restriction of the Brillouin zone sampling to the Γ point was found to give reliable results in a smaller zeolite unit cell.[31]

The density functional theory method allows to considerably speed up calculations. However, this has some consequences on the accuracy of the calculations. A known artifact stems from the poor capability of DFT to describe van der Waals contribution.[32,33] Adsorption energies when molecules are physisorbed are underestimated. We have described how to empirically correct the energies.[7] An alternative is to use an embedded method and to use a QM/QM description of the system, employing quantum methods that give a better description of the van der Waals contribution. This was achieved by several groups.[32−34] Concerning activation energy in chemical reaction, the limits of the density functional method are less dramatic as the errors compensate.[34] However, this generally leads to an underestimation on the order of 8 to 15 kJ/mol of activation energies in zeolite proton-exchanged, for instance.[34] As we will see, this does not change the predictive reaction pathways in this study, as the energy differences are beyond this limit.

The mordenite zeolite structure used in the calculations is similar to the one that has been used before.[7,8] The dimensions of the unit cell are $a = 13.648$ Å, $b = 13.672$ Å, $c = 15.105$ Å, $\alpha = 96.792°$, $\beta = 90.003°$, and $\gamma = 90.022°$. The Si/Al ratio in our mordenite model is 46. The Brønsted protonic site has been selected, as before, at the junction of twelve- and eight-member rings, as sites in this location are the more stable.[35,36] The position of the proton participating in the reaction has been selected to allow the formation of alkoxy species to the most accessible oxygen atom (i.e., at the junction of two eight-member rings). The alkoxy species is an important intermediate in the step-by-step reaction pathway as we will see later. The position of the proton around the aluminum is of less importance due to the relatively high mobility of proton in zeolite.[34,37] To avoid any interactions between a non-participating catalytic acidic site, only one Brønsted site was placed in the unit cell. The total number of atoms in the unit cell is 146. In the final optimized structures, there are no constraints or restraints on any atomic positions.

Relaxation of the adsorbed compounds and intermediates was performed employing a quasi-Newton algorithm based on analytical forces minimization. Convergence was assumed to be reached when all forces were below 0.05 eV/Å.

The transition state search method in VASP is the nudged elastic band method.[38] Several images of the system are defined along the investigated reaction pathway. These images are optimized but only allowed to move in the direction perpendicular to the vector defined by the hypertangent between their two neighboring images. We employed up to eight images to analyze potential energy surface in the surrounding of the transition states. When forces on the system images were below 0.08−0.10 eV/Å, the image with the maximum energy in the reaction pathway was separately optimized using force minimization with the same criteria as before.

## Results

Our reaction pathway choice for the step-by-step alkylation of benzene with propene follows experimental results as suggested in the study of Derouane et al.[18] It has been proposed that in order to achieve alkylation of benzene with propene, an excess of benzene with respect to propene should be used. This is believed to prevent side reactions between propene molecules. Derouane et al. propose that as soon as propene has been adsorbed in the zeolite micropores, it becomes protonated and chemisorbs to the zeolite wall. Then, alkylation of benzene follows. We designed our system the same way. Propene physisorbs to the Brønsted acidic site in the first step. After reaction of chemisorption, it is converted into alkoxy species. Then, benzene is put in contact with the propoxy species and an alkylation reaction takes place. The final intermediate in this reaction is cumene physisorbed to the Brønsted acidic site.

After propene has adsorbed within the zeolite mouth, it diffuses within the micropore and finally adsorbs to a Brønsted acidic site. Adsorption of olefin to the Brønsted site has been observed experimentally and theoretically to be energetically more favorable by around 20 kJ/mol than adsorption of olefin within an all silica zeolite micropore.[6,21] This energy is a good estimate of the affinity between olefin and the proton of the catalytic site.

Propene adsorbs via a $\eta^2$(C═C) mode with respect to the proton of the Brønsted acidic site. The geometry of propene physisorbed to the Brønsted acidic site is reported in Table 1. We previously achieved a study of this reaction in chabazite.[21] As the zeolite frameworks are different, the course of the reaction has no a priori reason to be similar. Results of the formation of isopropyl-MOR are compared with the previous calculations of the formation of isopropyl-CHA.[21] The position

**TABLE 1: Main Geometrical Parameters in Propene Chemisorption in Proton-Exchanged Mordenite and Chabazite: Details for Physisorbed (Ads_pro), Transition (TS_pro), and Chemisorbed (Alk_pro) States[a]**

| Ads_pro | MOR | CHA[b] | TS_pro | MOR | CHA[b] | Alk_pro | MOR | CHA[b] |
|---|---|---|---|---|---|---|---|---|
| $AlO_1$ | 1.90 | 1.90 | $AlO_1$ | 1.81 | 1.75 | $AlO_1$ | 1.71 | 1.69 |
| $AlO_2$ | 1.70 | 1.69 | $AlO_2$ | 1.72 | 1.73 | $AlO_2$ | 1.90 | 1.87 |
| $AlO_3$ | 1.69 | 1.67 | $AlO_3$ | 1.71 | 1.72 | $AlO_3$ | 1.71 | 1.69 |
| $AlO_4$ | 1.70 | 1.71 | $AlO_4$ | 1.71 | 1.72 | $AlO_4$ | 1.70 | 1.70 |
| $O_1H_a$ | 1.01 | 1.01 | $O_1H_a$ | 1.44 | 1.70 | | | |
| $O_1Si_1$ | 1.69 | 1.69 | $H_aC_1$ | 1.25 | 1.17 | | | |
| $O_2Si_2$ | 1.57 | 1.57 | $O_2C_2$ | 2.72 | 2.62 | $O_2C_2$ | 1.56 | 1.55 |
| $O_3Si_3$ | 1.56 | 1.57 | $O_1Si_1$ | 1.63 | 1.60 | $O_1Si_1$ | 1.58 | 1.57 |
| $O_4Si_4$ | 1.58 | 1.58 | $O_2Si_2$ | 1.57 | 1.58 | $O_2Si_2$ | 1.69 | 1.69 |
| $H_aC_1$ | 2.09 | 2.03 | $O_3Si_3$ | 1.57 | 1.57 | $O_3Si_3$ | 1.58 | 1.58 |
| $H_aC_2$ | 2.30 | 2.41 | $O_4Si_4$ | 1.57 | 1.58 | $O_4Si_4$ | 1.58 | 1.59 |
| $AlO_1Si_1$ | 133.2 | 127.3 | $AlO_1Si_1$ | 132.4 | 146.0 | $AlO_1Si_1$ | 132.9 | 133.0 |
| $AlO_2Si_2$ | 142.2 | 142.3 | $AlO_2Si_2$ | 141.2 | 136.8 | $AlO_2Si_2$ | 128.0 | 125.6 |
| $AlO_3Si_3$ | 150.4 | 162.1 | $AlO_3Si_3$ | 148.0 | 139.1 | $AlO_3Si_3$ | 144.0 | 159.7 |
| $AlO_4Si_4$ | 153.1 | 152.5 | $AlO_4Si_4$ | 160.0 | 144.2 | $AlO_4Si_4$ | 166.3 | 143.7 |
| $AlO_1H_a$ | 111.5 | 115.1 | $AlO_1H_a$ | 31.8 | 103.9 | $AlO_2Si_2C_2$ | −176.6 | 178.5 |
| $AlO_1Si_1H_a$ | −159.2 | 157.7 | $O_1H_aC_1$ | 175.7 | 173.5 | | | |
| | | | $AlO_2C_2$ | 45.3 | 114.4 | | | |
| | | | $AlO_1Si_1H_a$ | −0.7 | − | | | |

[a] Distances in Å, and angles in degrees. [b] Ref 21.

**SCHEME 1: Reaction Mechanisms in the Step-by-Step Alkylation of Benzene with Propene Catalyzed by Proton-Exchanged Zeolite Leading to the Formation of Cumene[a]**

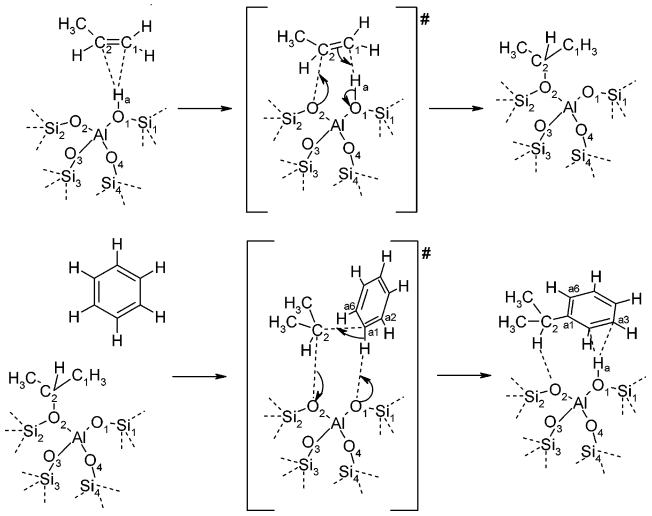

[a] Labels are the same as used in Tables 1 and 2.

of the propene carbon−carbon double bond is located qualitatively the same with respect to the proton in mordenite and in chabazite.

Once propene gets in contact with the acidic site, it becomes easily protonated. Experimental results report that this occurs readily at room temperature.[18]

In the chemisorption transition state, propene gets protonated in $C_1$ whereas the carbon atom $C_2$ is being chemically bonded with an oxygen atom of the catalytic site (see Scheme 1). The main geometrical parameters of the transition states when this reaction is catalyzed by mordenite and chabazite are reported in Table 1. One can see that the geometries of the transition states in mordenite and in chabazite are very similar.

The activation energy for this reaction was 56 kJ/mol in chabazite.[21] The calculations achieved here give a similar activation energy barrier. We find an activation energy of 60 kJ/mol. This activation energy is slightly higher in mordenite than in chabazite.

The chemisorption of propene leads to the formation of an alkoxy species. The reaction energy for this step is exothermic.[18] Here, we find a reaction energy of −25 kJ/mol. This value is in good agreement with that obtained before. For a reaction in chabazite, we found a reaction energy of −27 kJ/mol.[21] This means that isoproxide does not suffer from steric constraints in its contact with the zeolite walls in mordenite and in chabazite. The main geometrical parameters of the isopropoxy species in mordenite as obtained in this study and in chabazite as obtained in the previous study are reported in Table 1. Similar geometries are found.

We consider only the more favorable protonation product in this study. In principle, propene can get protonated in the $C_1$ or $C_2$ position (see Scheme 1). However, it is well known that the formation of *n*-propoxy species is unlikely.[21] This is mainly because it necessitates the formation of a primary carbocation that is more energetically demanding than the formation of a secondary carbocation.[21,39] Actually, *n*-propoxide is an unlikely product not because of the reaction energy, which is similar to that of *i*-propoxide formation, but because of the high energy that is required to reach primary carbocation-like transition state.

Propene chemisorption is the first step in the step-by-step alkylation of benzene with propene, which leads to the formation of cumene. Alkylation of benzene with propene can occur when benzene physisorbs close to *i*-propoxide. We checked different configurations of benzene with respect to the alkoxy species and mordenite micropore. The different configurations are shown in Figure 1. Benzene has been considered as adopting perpendicular and parallel orientations with respect to the direction of the main channel. We observe here that when the $C_2$ symmetry axis of benzene is parallel to the direction of the mordenite channel the energy is lower (see (a) in Figure 1). When the $C_2$ symmetry axis of benzene is perpendicular to the direction of the main micropore direction, the adsorption mode is less favorable with an energy of +33 kJ/mol with respect to the previous adsorption mode (see (b) in Figure 1). A third adsorption mode for benzene has been considered (see (c) in Figure 1). In this last case, benzene interacts with the *i*-propoxy species. The energy for this system is +7 kJ/mol with respect to the energy of the system in which benzene is oriented parallel to the direction of the mordenite channel.

After benzene has adsorbed in a nearby location to the alkoxy species, alkylation takes place. We investigated different reaction pathways leading to the same reaction. For this purpose, we used up to eight images of the system along slightly different

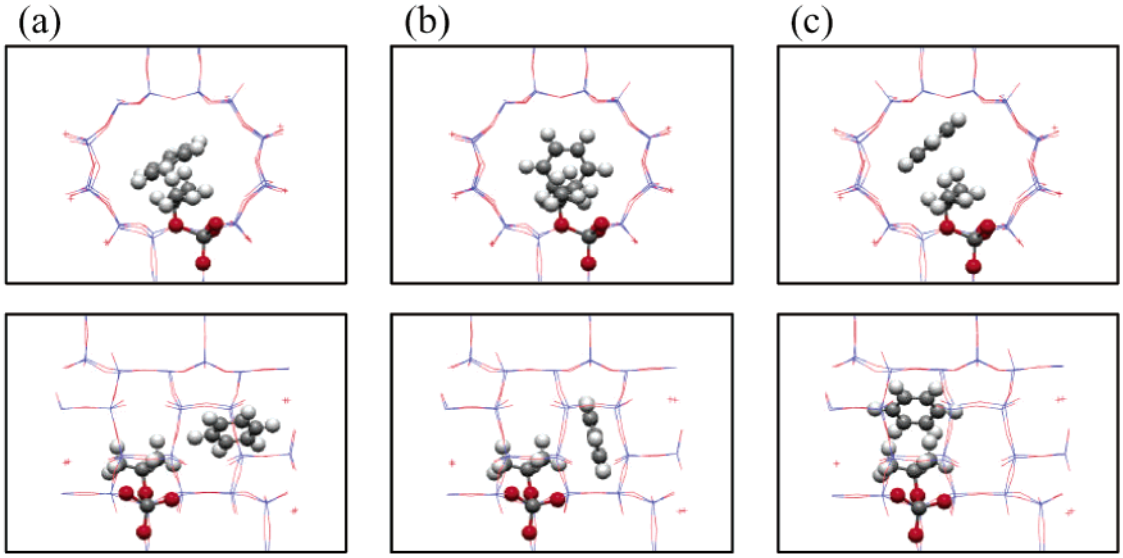


**Figure 1.** Front and side views of the geometries of the different adsorption modes of benzene physisorbed in propoxy mordenite.

**TABLE 2: Main Geometrical Parameters for Step-by-Step Alkylation of Benzene with Propene Catalyzed by Proton-Exchanged Mordenite: Details for Benzene Physisorbed to Propoxide (Ads_benz, alk), Transition (TS_alky), Charged Intermediate (Int), and Physisorbed Cumene (Ads_cumene) States**[a]

| Ads_benz alk | | TS_alky | | Int | | Ads_cumene | |
|---|---|---|---|---|---|---|---|
| $AlO_1$ | 1.71 | $AlO_1$ | 1.73 | $AlO_1$ | 1.73 | $AlO_1$ | 1.90 |
| $AlO_2$ | 1.89 | $AlO_2$ | 1.73 | $AlO_2$ | 1.73 | $AlO_2$ | 1.69 |
| $AlO_3$ | 1.71 | $AlO_3$ | 1.74 | $AlO_3$ | 1.75 | $AlO_3$ | 1.69 |
| $AlO_4$ | 1.69 | $AlO_4$ | 1.72 | $AlO_4$ | 1.72 | $AlO_4$ | 1.71 |
| $O_2C_2$ | 1.56 | $O_1Si_1$ | 1.57 | $O_1Si_1$ | 1.57 | $H_aO_1$ | 1.00 |
| $O_1Si_1$ | 1.58 | $O_2Si_2$ | 1.56 | $O_2Si_2$ | 1.56 | $H_aC_{a3}$ | 2.18 |
| $O_2Si_2$ | 1.68 | $O_3Si_3$ | 1.57 | $O_3Si_3$ | 1.57 | $H_aC_2$ | 2.45 |
| $O_3Si_3$ | 1.58 | $O_4Si_4$ | 1.57 | $O_4Si_4$ | 1.56 | $O_1Si_1$ | 1.69 |
| $O_4Si_4$ | 1.58 | $AlO_1Si_1$ | 139.7 | $AlO_1Si_1$ | 140.9 | $O_2Si_2$ | 1.57 |
| $AlO_1Si_1$ | 138.4 | $AlO_2Si_2$ | 149.8 | $AlO_2Si_2$ | 148.8 | $O_3Si_3$ | 1.56 |
| $AlO_2Si_2$ | 129.0 | $AlO_3Si_3$ | 141.6 | $AlO_3Si_3$ | 140.0 | $O_4Si_4$ | 1.58 |
| $AlO_3Si_3$ | 145.0 | $AlO_4Si_4$ | 158.9 | $AlO_4Si_4$ | 159.4 | $AlO_1Si_1$ | 131.9 |
| $AlO_4Si_4$ | 166.0 | $C_2C_{a1}$ | 1.73 | $C_2C_{a1}$ | 1.70 | $AlO_2Si_2$ | 142.8 |
| $AlO_2Si_2C_2$ | −179.0 | $H_2O_2$ | 2.20 | $H_2O_2$ | 2.33 | $AlO_3Si_3$ | 154.1 |
| | | $H_2C_2C_{a1}C_{a2}$ | 172.0 | $H_2C_2C_{a1}C_{a2}$ | 173.8 | $AlO_4Si_4$ | 152.8 |
| | | $C_{a2}C_{a1}C_{a6}C_2$ | −116.7 | $C_{a2}C_{a1}C_{a6}C_2$ | −122.0 | $AlO_1Si_1H_a$ | −158.4 |
| | | $C_{a2}C_{a1}C_{a6}H_{a1}$ | −138.2 | $C_{a2}C_{a1}C_{a6}H_{a1}$ | −132.7 | $C_2C_{a1}$ | 1.52 |
| | | | | $H_{a1}O_3$ | 2.37 | $H_2O_3$ | 3.33 |
| | | | | $C_{a1}H_{a1}$ | 1.11 | $H_2C_2C_{a1}C_{a2}$ | −54.3 |

[a] Distances in Å, and angles in degree.

reaction pathways using the nudge elastic band method.[38] The energy of these systems was minimized until forces were below a limit of around 0.1 eV/Å. The different reaction pathways were compared to each other. The reaction pathway with the smaller higher energy was further minimized. This method was used to eliminate any steric constraints between the complex transition state structure and the zeolite wall.

The main geometrical parameters of the alkylation of benzene with propyl transition state are reported in Table 2. The activation energy with respect to benzene physisorbed in a nearby position to the alkoxy species is $E_{act} = 38$ kJ/mol. This energy is evaluated with respect to the physisorbed system that has the lowest energy (see (a) in Figure 1). In the transition state, the propyl secondary carbocation can be considered as a distorted carbocation (see Figure 2). The cleavage of the alkoxy bond between the propyl fragment and the zeolite oxygen atom is not part of the alkylation transition state mechanism. However, propyl is rather far from a "pure" carbocation as the dihedral angle $H_2C_2C_3C_1$ is 28.9°, whereas it is expected to be around 0° in a secondary carbocation. The chemical bond between the benzene and the propyl is in formation as indicated by the $C_2C_{a1}$ distance ($C_2C_{a1} = 1.73$ Å, see in Table 2). One notes that the hydrogen on $C_{a1}$ is not back-donated to the deprotonated Brønsted sites in this step. The proton back-donation takes place after the product of the alkylation reaction step is formed. To achieve proton back-donation, the cumene carbocation needs to reorient itself in order to present its exceeding proton in a favorable situation.[20] One notes that the alkoxy bond between the propyl molecular fragment and the zeolite oxygen atom is broken prior the transition state being reached.

The carbocation that is reached after alkylation of benzene with propene has been optimized. We started from the transition state structure and performed a dynamic annealing simulation without putting any constraint on the system. The transition state quickly evolved toward a carbocationic species. Then this system was minimized employing the same method and criteria as before. The geometry of this system is reported in Table 2. It corresponds to an intermediate in the reaction pathway.[41] The comparison of its geometry with that of the alkylation transition state reveals how close the nature of the transition state is to that of a carbocation. Distances, angles, and dihedral angles in the transition state and in the carbocation are related. Energy

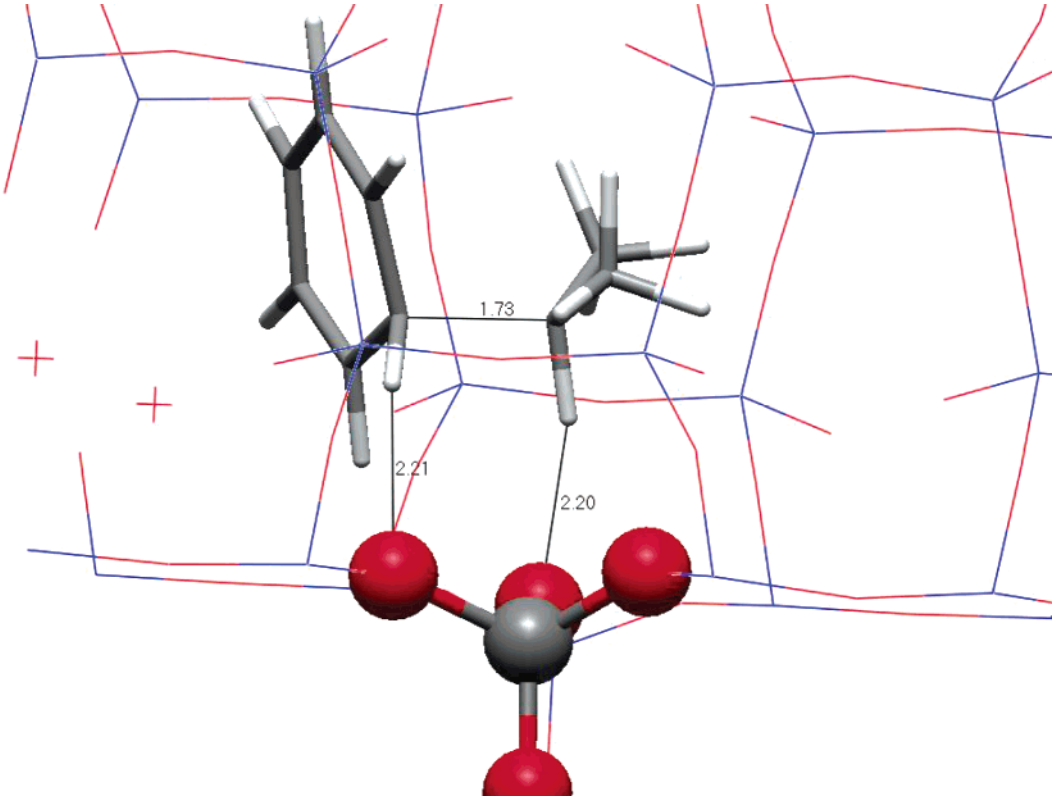


**Figure 2.** Geometry details in the reaction transition state of alkylation of benzene with propene catalyzed by mordenite. See TS_alky in Table 2.

of the carbocation is +26 kJ/mol with respect to benzene physisorbed to the alkoxy species. This is 11 kJ/mol more stable than the transition state. As observed also in the methylation of toluene with methanol,[20] the carbocation that is formed after alkylation of benzene with propene shows some stability. However, according to the results of Nicholas and Haw[42] and Bjørgen et al.,[43] this cation should not be stable enough to be experimentally observed in protonic zeolite. The theoretical model developed by Nicholas and Haw[42] explains this result.

After proton back-donation from the carbocation has occurred, the catalytic reaction is completed. The Brønsted acidic site is restored and cumene is formed. The main geometrical parameters of this system are summarized in Table 2 (see Ads_cumene). The energy computed for this system is −70 kJ/mol with respect to the energy of benzene adsorbed to isoproxy species in mordenite. This energy is relatively important but is indeed in the range of the experimental and theoretical reaction energy of cumene formation from benzene and propene.[44,45]

The associative reaction pathway of alkylation of benzene with propene has also been investigated. Protonation of propene with the Brønsted acidic site proton and alkylation of benzene with the propyl carbocation being formed occurs simultaneously when the transition state structure is reached in this reaction pathway (see Scheme 2).

The associative alkylation of benzene with propene requires that propene physisorbs to the zeolitic Brønsted site, whereas benzene is located in the surrounding (see Figure 4a). The presence of benzene does not affect much the physisorbtion of propene, as can be seen when the details of the geometry of the system are compared with that of physisorbtion of propene in the absence of benzene (see Tables 1 and 3).

The Brønsted acidic site proton attacks $C_1$ in propene in the transition state structure (see Figure 4b and Table 3). The zeolite oxygen atom−proton bond is already clearly broken as is shown by the distance between these two atoms ($O_1H_a$ = 2.04 Å). The

**SCHEME 2: Reaction Mechanisms in the Associative Alkylation of Benzene with Propene Catalyzed by Proton-Exchanged Zeolite Leading to the Formation of Cumene**[a]

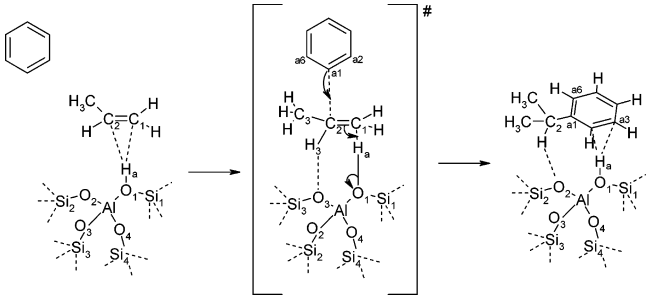

[a] Labels are the same as used in Table 3.

olefin carbon atom−proton bond is very close to being completely formed. The distance between these atoms is 1.13 Å. A carbon−hydrogen bond distance is expected to be 1.09 Å (see, for instance, $C_2H_3$ in Table 3).

The $C_1C_3H_3C_2$ plane is already bended, indicating the change in hybridization of the olefin carbon atom from C-sp2 to C-sp3 (See Table 3). The same holds for the $C_3C_1H_3C_2$ plane. On the other hand, the benzene structure is still little affected in the transition state structure: the dihedral angle $C_{a6}C_{a2}H_{a1}C_{a1}$ remains very close to that of stable structure (see Table 3). Other important geometrical parameters of the transition state structures can be found in Table 3. Comparison of this transition state structure with the one that has been found in the cluster approach study[44,45] reveals that it is definitively closer to the transition state structure of alkylation of benzene with ethene than to the transition state structure of alkylation of benzene with propene. The latter seems to be actually similar to the step-by-step transition state that we have found in the present study. The geometry of the direct reaction pathway alkylation transition

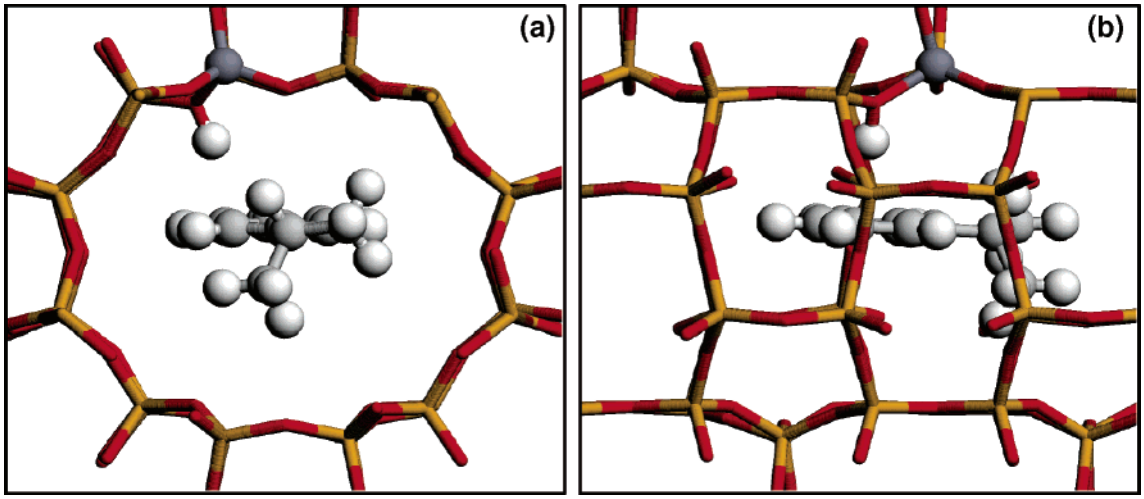


**Figure 3.** Front and side views of cumene adsorbed in proton-exchanged mordenite.

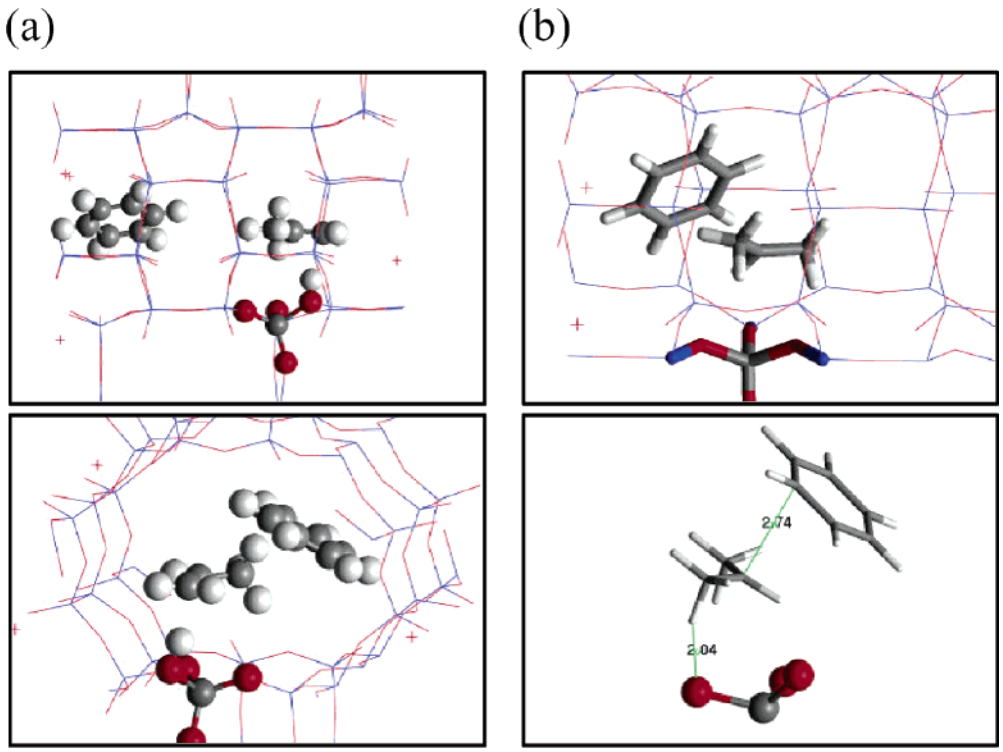


**Figure 4.** Front and side views of the geometries of propene physisorbed to the Brønsted acidic site and benzene (a) and of the direct alkylation transition state of benzene with propene (b) in mordenite.

state can be seen in Figure 4b. The activation energy that is required to reach this structure is 37 kJ/mol. This activation energy is close to that of the alkylation of benzene with propene in the step-by-step pathway.

The product of this reaction is similar to that in the step-by-step reaction pathway. The same carbocationic intermediate as before is reached. This intermediate evolves toward a restored catalytic site and cumene. Cumene is physisorbed to the zeolite acidic proton (see Figure 3). The energy of this system is −92 kJ/mol with respect to propene physisorbed to the Brønsted acidic site and benzene in a nearby position (see Figure 4a).

## Discussion

When compared with cluster approach studies of the same reaction,[44,45] our periodic density functional study of the alkylation of benzene with propene reveals several interesting facts. The reaction energy diagrams of the two reaction routes are reported in Figure 5. As observed earlier, activation energies decrease in comparison with cluster approach calculations when the bulk periodical structure is considered.[16] This stabilization energy is not uniform here and changes completely the reaction energy diagrams of the reactions as they have been previously described.[44,45]

We observe that the protonation and chemisorption of propene is more difficult to achieve than both alkylation of benzene with propene and alkylation of benzene with propoxide. This was not the case in the cluster approach study: the activation energy for the chemisorption of propene was clearly easier than the alkylation of benzene with propene.[44,45] The activation energies of the alkylation reaction steps in the associative and in the step-by-step (i.e., once the formation of propoxide is achieved) reaction pathways are similar. In the cluster approach study, the direct alkylation was slightly preferred.[44] One can expect, as suggested in the NMR study of cumene formation catalyzed

**TABLE 3: Main Geometrical Parameters for Direct Alkylation of Benzene with Propene Catalyzed by Proton-Exchanged Mordenite: Details for Propene Physisorbed to the Brønsted Acidic Site in Presence of Benzene (Ads_prop_benz), and the Direct Alkylation Transition (TS_alky2) States[a]**

| Ads_prop_benz | | TS_alky2 | | | |
|---|---|---|---|---|---|
| $AlO_1$ | 1.90 | $AlO_1$ | 1.76 | $H_3O_3$ | 2.16 |
| $AlO_2$ | 1.69 | $AlO_2$ | 1.73 | $C_1C_2H_3$ | 115.6 |
| $AlO_3$ | 1.69 | $AlO_3$ | 1.73 | $C_2H_3O_3$ | 134.2 |
| $AlO_4$ | 1.70 | $AlO_4$ | 1.71 | $AlO_1H_aC_1$ | 37.2 |
| $O_1Si_1$ | 1.69 | $O_1Si_1$ | 1.58 | $H_aC_1C_2C_{a1}$ | −170.7 |
| $O_2Si_2$ | 1.56 | $O_2Si_2$ | 1.57 | $C_2H_1H_2C_1$ | −26.6 |
| $O_3Si_3$ | 1.57 | $O_3Si_3$ | 1.56 | $C_3C_1H_3C_2$ | 12.0 |
| $O_4Si_4$ | 1.58 | $O_4Si_4$ | 1.57 | $C_{a6}C_{a2}H_{a1}C_{a1}$ | 2.2 |
| $O_1H_a$ | 1.01 | $AlO_1Si_1$ | 139.0 | $C_2H_4H_6C_3$ | −30.4 |
| $H_aC_1$ | 2.09 | $AlO_2Si_2$ | 140.3 | | |
| $H_aC_2$ | 2.29 | $AlO_3Si_3$ | 152.2 | | |
| $AlO_1Si_1$ | 133.2 | $AlO_4Si_4$ | 155.6 | | |
| $AlO_2Si_2$ | 111.7 | $O_1H_a$ | 2.04 | | |
| $AlO_3Si_3$ | 150.5 | $H_aC_1$ | 1.13 | | |
| $AlO_4Si_4$ | 142.3 | $O_1H_aC_1$ | 151.0 | | |
| $O_1H_aC_1$ | 165.2 | $H_aC_1C_2$ | 97.1 | | |
| $O_1H_aC_2$ | 154.4 | $C_1C_2C_{a1}$ | 101.6 | | |
| $O_1H_aC_1C_2$ | −139.7 | $C_2C_{a1}$ | 2.74 | | |
| | | $C_2H_3$ | 1.09 | | |

[a] Distances in Å, and angles in degree.

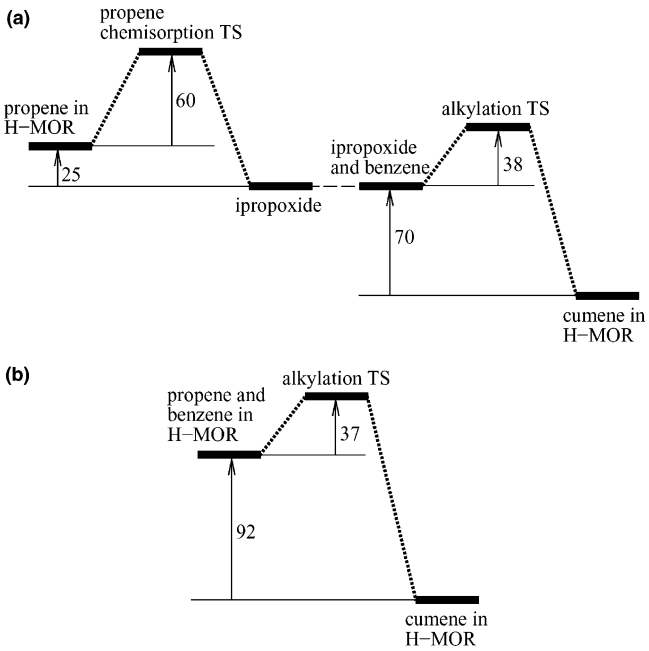


**Figure 5.** Reaction energy diagrams of (a) the step-by-step alkylation and (b) the direct alkylation of benzene with propene catalyzed by acidic mordenite. All values in kJ/mol.

by H−ZSM-11 of Derouane et al.,[18] that in the case where benzene is present in large excess compared to propene, the consecutive reaction pathway becomes dominant.

The simple relationship between activation energy and the type of intermediate transition state carbocation, and especially the order of the hydrocarbon cation, was a key to the concept of transition state selectivity in zeolite-catalyzed reactions. Alkylation of benzene with propene can be used as an illustration of this concept.

Propene is readily protonated in acidic zeolite.[18] This is not the case for benzene, which is more difficult to protonate.[18] Thermodynamic considerations can easily explain this result.[46] The aromaticity of benzene is of course the main reason. Protonation of propene leads to two possible carbocations.[18,21] The activation energy to protonate propene relates to the stability of the charged intermediate. As previously discussed, formation of a primary carbocation is unlikely and hence formation of a secondary carbocation is much more easily achieved. Then, cumene is preferentially formed in protonic zeolite rather than *n*-propyl benzene. This later product can be formed in zeolite when isomerization takes place.[18]

Recently, Vos et al.[44] studied the same reaction as described here using a cluster approach method. They have proposed that the alkoxy species would induce too large geometry modifications in the cluster geometry to be a stable intermediate. They estimated that in real zeolites such large geometry changes could not be accommodated by the zeolite framework. In periodic density functional studies, we are able to check whether alkoxy species can exist in realistic zeolite models.

In the current study, the energy of the alkoxide is also found to be similar to those obtained in unconstrained cluster approach calculations. The reaction energy of propene chemisorption in mordenite is −25 kJ/mol (see Figure 5). Vos et al.[44] found a reaction energy of −50 kJ/mol. Senger and Radom[39] and Sinclair et al.[47] found reaction energies of −28 kJ/mol and −49 kJ/mol, respectively. Therefore, it appears that the large geometry changes in the zeolite framework that are induced because of the alkoxide formation can be accommodated without high energy fluctuation by the zeolite framework. We observed that the critical parameter in the study of chemisorbed olefin in zeolite is the zeolite model, and especially the degree of relaxation that is allowed in the system.[21] Any constraints on zeolite atom positions induce erroneous results and destabilization of the energy of alkoxy species.[21,48] This is explained by the covalent nature of chemical bonds in alkoxy species and zeolite.[6,16,49]

To support the fact that isopropoxide may not be stable in zeolite, Vos et al.[44] mentioned the studies of Milas and Nascimento,[50] Ivanova and Corma,[51] and Mirth and Lercher.[52] However, these studies concern isobutene chemisorption (isobutane dehydrogenation). With isobutene, a tertiary carbocation is formed after protonation. Sinclair et al.[47] and Rozanska et al.[22] have shown in quantum chemical studies that other factors may become important in the case of isobutoxide. Moderate to strong steric constraints between the methyl groups in the alkoxy species and the zeolite walls can significantly modify the stability of alkoxy species.

Now, let us go back on some of the fundamental concepts that have been developed these last years. Then, the other apparently contradictory activation energies for the different reactions obtained in the present study when compared to cluster approach study[44,45] are explained. The most striking mismatch with previous results is that the relative order between olefin chemisorption and alkylation with olefin is strongly altered.[16,44] Direct alkylation of benzene with propene becomes clearly more favorable than propene chemisorption (see Figure 5). The cluster approach calculations predict only a small preference for the direct alkylation route.[44]

It is known since the work of Ramachandran et al.[53] and Rozanska et al.[7,54] that "larger" transition states are more stabilized by the zeolite framework oxygen atoms: a larger carbocationic transition state interacts with more oxygen atoms and therefore is more likely to be more stabilized by the zeolite host. Also, it was noted that a strong electron delocalization occurred: the limitation of the zeolite catalyst to a molecular fragment is then biased. This is according to Ramachandran et al.[53] the main reason why associative reaction mechanisms rather than consecutive reaction mechanisms are usually more likely

in zeolite. Of course, one cannot find this when doing quantum chemical calculations employing the cluster approach of these reactions, as the zeolite catalyst cavity is not explicitly considered.[16] This may explain why Vos et al.[44] could not make a clear distinction between the activation energies of propene protonation/chemisorption and benzene alkylation with propene.[16,44] As both transition states are propenium carbocation-like transition states, the activation energies for these two reactions is of the same order in the cluster approach method. However, the effect of the zeolite framework on a transition state complex is important and changes this result, as shown in the present study.

Let us go back to a short description of the parameters that would induce molecular recognition of a guest molecule by the host structure. First, the lock and key concept is associated with an ideal geometrical fit between the lock and key structures. Second, the electronic signature of the key or guest molecule has to agree with the electronic signature of the lock or host structure. Electronic density adapts itself to the shape of the carbocationic reaction transition state.[7,54] Also, as the size of the transition state increases, energy stabilization of the reaction transition state complex becomes more important and can even lead to different reaction paths.[54] We noted in our previous quantum chemical calculations[7,8,54] that transition state energy stabilization by the zeolite framework in comparison with cluster approach calculations relates to the charge separation in the transition state complex. Less charge separation implies less transition state structure stabilization by the zeolite host. Last, entropy−enthalpy compensation should be taken into account for a correct prediction in computational chemistry.[41b] This was not considered in the present study. The diminution of the degree of freedom of the guest molecule upon contact with the host molecule may lead to a decrease of entropy.[55,56] An ideal balance has to be obtained between entropy loss and enthalpy gain in the interaction of guest−host system.[41b] Enthalpy−entropy compensation similar to that in biological systems has been observed in zeolite, as, for instance, in adsorption studies of alkanes in zeolite micropores[9,10] and in the disproportionation reaction between *m*-xylene catalyzed by FAU, MFI, and MOR.[41b]

In the present study, one finds an activation energy for propene protonation of 60 kJ/mol (see Figure 5). We observed an activation energy of 57 kJ/mol in chabazite zeolite.[21] The activation energy is slightly lower in chabazite in comparison with that of in mordenite. We obtained similar results in a study of isobutene chemisorption in chabazite, ZSM-22, and mordenite.[22] This is due to the better contact of the transition state complex with the zeolite framework, which enhances transition state complex stabilization by the zeolite framework. In cluster approach calculations,[44] activation energies around 124 kJ/mol with respect to propene physisorbed to a zeolite molecular fragment are reported.

Next, we investigated the alkylation of benzene by the propyl alkoxy intermediate (step-by-step reaction pathway) and by propene (associative reaction pathway). The activation energy barriers for these reaction mechanisms are 38 kJ/mol and 37 kJ/mol, respectively. In the chemisorption of the propene transition state, and as observed in cluster approach calculations,[44] protonation of propene has occurred. Activation energies of 124 kJ/mol with respect to benzene and propene physisorbed to a zeolite molecular fragment are reported.[44]

The energy of the propene chemisorption transition state is reduced by 64 kJ/mol in its contact with the zeolite framework compared with cluster approach calculations. In the cluster approach transition state complex, the Mulliken charge of the transition state complex has been estimated to be around +0.6. The Mulliken charge for the alkylation of benzene with propene transition state complex is around +1. The reduction of the activation energy between cluster approach calculation and periodic density functional theory calculation from a reaction starting from isopropoxide and benzene is around 137 kJ/mol. The same energy stabilization is obtained when the associative reaction pathway is followed.

## Conclusions

We have performed a periodic quantum chemical investigation of alkylation of benzene with propene catalyzed by proton-exchanged mordenite. In this study, the contradictions in the comparison between previous cluster approach studies and the present electronic periodic structure calculation results confirm that zeolite catalyst operates through a lock and key type mechanism.[22,54,57] The preferential formation of particular transition state complexes in a zeolite-catalyzed reaction obeys simple rules. Preference to a particular complex relates to the relative stability of the corresponding carbocationic structures and the energy cost involved in the charge separation between the carbocation and the zeolite framework in the transition state. However, the zeolite framework can also modify these simple rules. The stabilization energy of transition state complexes by the zeolite framework also depends on the size and shape of the carbocationic transition state complexes with respect to the zeolite framework. The stabilization energy becomes larger when more zeolite oxygen atoms can get into contact with the carbocationic transition state. This explains why the alkylation transition states have lower energies than that of the propene protonation/chemisorption. The cluster approach method does not describe the zeolite framework and is therefore unable to predict this trend.

Considering the energies that are involved in the reaction, it is clear that the alkylation of benzene catalyzed by proton-exchanged zeolite occurs readily. Direct alkylation of benzene with propene is preferred versus the consecutive path, since the activation energy barrier to protonate propene for the latter is significantly higher.

**Acknowledgment.** Computational resources were granted by the Dutch National Computer Facilities (NCF) and the Technical University of Eindhoven. This work was performed within the European Research Group "Ab Initio Molecular Dynamics Applied to Catalysis", supported by CNRS, IFP, and Total.

## References and Notes

(1) Barrer, R. M. *Zeolite and Clay Minerals as Sorbents and Molecular Sieves*; Academic Press: New York, 1978.

(2) (a) Breck, D. *Zeolite Molecular Sieves, Structure, Chemistry and Use*; Wiley: New York. (b) Che, M.; Clause, O.; Marcilly, C. *Handbook of Heterogeneous Catalysis*; Ertl, G., Knözinger, H., Weitkamp, J., Eds.; Wiley-VCH: Weinheim, 1997; p 191.

(3) (a) Fricke, R.; Kosslick, H.; Lischke, G.; Richter, M. *Chem. Rev.* **2000**, *100*, 2303. (b) Venuto, P. B. *Microporous Mater.* **1994**, *2*, 297.

(4) (a) Campanati, M.; Fornasari, G.; Vaccari, A. *Catal. Today* **2003**, *77*, 299. (b) Thomas, J. M.; Thomas, W. J. *Principles and Practice of Heterogeneous Catalysis*; VCH: Weinheim, 1997; p 6.

(5) (a) Chen, N. Y.; Degnan, T. F., Jr.; Smith, C. M. *Molecular Transport and Reaction in Zeolites, Design and Application of Shape Selective Catalyst*; VCH Publishers: New York, 1994. (b) Csicsery, S. M. *Zeolites* **1984**, *4*, 202. (c) Fraenkel, D.; Levy, M. *J. Catal.* **1989**, *10*, 118.

(6) Van Santen, R. A.; Rozanska, X. *Adv. Chem. Eng.* **2001**, *28*, 399.

(7) Rozanska, X.; Van Santen, R. A.; Hutschka, F.; Hafner, J. *J. Am. Chem. Soc.* **2001**, *123*, 7655.

(8) Rozanska, X.; Van Santen, R. A.; Hutschka, F. *J. Phys. Chem. B* **2002**, *106*, 4652.
(9) Bates, S. P.; Van Well, W. J. M.; Van Santen, R. A.; Smit, B. *J. Am. Chem. Soc*. **1996**, *118*, 6753.
(10) Bates, S. P.; Van Santen, R. A. *Adv. Catal*. **1998**, *42*, 1.
(11) (a) Yashonath, S.; Santikary, P. *J. Phys. Chem*. **1993**, *97*, 3849. (b) Yashonath, S.; Santikary, P. *Mol. Phys*. **1993**, *78*, 1. (c) Yashonath, S.; Santikary, P. *J. Chem. Phys*. **1994**, *100*, 4013.
(12) Baerlocher, C.; Meier, W. M.; Olson, D. H. *Atlas of Zeolite Framework*; Elsevier: Amsterdam, 2001.
(13) Kazansky, V. B.; Senchenya, I. N. *J. Catal*. **1989**, *108*, 119.
(14) Karplus, M.; Kushick, J. *Macromol*. **1981**, *14*, 325.
(15) Van Santen, R. A.; Niemantsverdriet, J. W. *Chemical Kinetics and Catalysis*; Plenum Press: New York, 1995.
(16) Rozanska, X.; Van Santen, R. A. *Handbook of Zeolite Technology and Science*; Auerbach, S. M., Carrado, K. A., Dutta, P. K., Eds.; Marcel Dekker: New York, 2003; p 785.
(17) (a) Eyring, H. *Trans. Faraday Soc*. **1938**, *34*, 1. (b) Wigner, E. *Trans. Faraday Soc*. **1938**, *34*, 29.
(18) Derouane, E. G.; He, H.; Hamid, S. B. D.-A.; Ivanova, I. I. *Catal. Lett*. **1999**, *58*, 1.
(19) Becker, K. A.; Karge, H. G.; Strenbel, W. D. *J. Catal*. **1973**, *28*, 403.
(20) Vos, A. M.; Rozanska, X.; Schoonheydt, R. A.; Van Santen, R. A.; Hutschka, F.; Hafner, J. *J. Am. Chem. Soc*. **2001**, *123*, 2799.
(21) Rozanska, X.; Demuth, T.; Hutschka, F.; Hafner, J.; Van Santen, R. A. *J. Phys. Chem. B* **2002**, *106*, 3248.
(22) Rozanska, X.; Van Santen, R. A.; Demuth, T.; Hutschka, F.; Hafner, J. *J. Phys. Chem. B* **2003**, *107*, 1309.
(23) Demuth, T.; Rozanska, X.; Benco, L.; Hafner, J.; Van Santen, R. A.; Toulhoat, H. *J. Catal*. **2003**, *214*, 68.
(24) Kresse, G.; Hafner J. *Phys. Rev. B* **1993**, *48*, 13115.
(25) Kresse, G.; Hafner, J. *Phys. Rev. B* **1994**, *49*, 14251.
(26) Kresse, G.; Furthmüller, J. *Comput. Mater. Sci*. **1996**, *6*, 15.
(27) Kresse, G.; Furthmüller, J. *Phys. Rev. B* **1996**, *54*, 11169.
(28) Perdew, J. P.; Zunger, A. *Phys. Rev. B* **1981**, *23*, 5048.
(29) Perdew, J. P.; Burke, K.; Wang, Y. *Phys. Rev. B* **1996**, *54*, 16533.
(30) Kresse, G.; Hafner, J. *J. Phys.: Condens. Matter* **1994**, *6*, 8245.
(31) Jeanvoine, Y.; Angyan, J.; Kresse, G.; Hafner, J. *J. Phys. Chem. B* **1998**, *102*, 5573.
(32) Pelmenschikov, A.; Leszcynski, J. *J. Phys. Chem. B* **1999**, *103*, 6886.
(33) Ugliengo, P.; Damin, A. *Chem. Phys. Lett*. **2002**, *366*, 683.
(34) Tuma, C.; Sauer, J. *Chem. Phys. Lett*. **2004**, *387*, 388.
(35) Demuth, T.; Benco, L.; Hafner, J.; Toulhoat, H.; Hutschka, F. *J. Chem. Phys*. **2001**, *114*, 3703.
(36) Brändel, M.; Sauer, J. *J. Am. Chem. Soc*. **1998**, *120*, 1556.
(37) Sauer, J.; Sierka, M.; Haase, F. *Transition State Modeling for Catalysis*; Truhlar, D. G., Morokuma, K., Eds.; *ACS Symp. Ser*. No 721; American Chemical Society: Washington, DC, 1999; p 358.
(38) Mills, G.; Jónsson, H.; Schenter, G. K. *Surf. Sci*. **1995**, *324*, 305.
(39) Senger, S.; Radom, L. *J. Am. Chem. Soc*. **2000**, *122*, 2613.
(40) Demuth, T.; Hafner, J.; Benco, L.; Toulhoat, H. *J. Phys. Chem. B* **2000**, *104*, 4593.
(41) (a) Clark, L. A.; Sierka, M.; Sauer, J. *J. Am. Chem. Soc*. **2003**, *125*, 2136. (b) Clark, L. A.; Sierka, M.; Sauer, J. *J. Am. Chem. Soc*. **2004**, *126*, 936.
(42) Nicholas, J. B.; Haw, J. F. *J. Am. Chem. Soc*. **1998**, *120*, 11804.
(43) Bjørgen, M.; Bonino, F.; Kolboe, S.; Lillered, K.-P.; Zecchina, A.; Bordiga, S. *J. Am. Chem. Soc*. **2003**, *125*, 15863.
(44) Vos, A. M.; Schoonheydt, R. A.; De Proft, E.; Geerlings, P. *J. Phys. Chem. B* **2003**, *107*, 2001.
(45) Arstad, B.; Kolboe, S.; Stein, O. *J. Phys. Chem. B* **2004**, *108*, 2300.
(46) Paukshtis, E. A.; Malyshera, L. V.; Stepanov, V. G. *React. Kinet. Catal. Lett*. **1998**, *65*, 145.
(47) Sinclair, P. E.; De Vries, A.; Sherwood, P.; Catlow, C. R. A.; Van Santen, R. A. *J. Chem. Soc., Faraday Trans*. **1998**, *94*, 3401.
(48) Boronat, M.; Viruela, P. M.; Corma, A. *J. Am. Chem. Soc*. **2004**, *126*, 3300.
(49) Van Santen, R. A.; Kramer, G. J. *Chem. Rev*. **1995**, *95*, 637.
(50) Milas, I.; Nascimento, M. A. C. *Chem. Phys. Lett*. **2001**, *338*, 67.
(51) Ivanova, I. I.; Corma, A. *J. Phys. Chem. B* **1997**, *101*, 547.
(52) (a) Mirth, G.; Lercher, J. A. *J. Phys. Chem*. **1991**, *95*, 3736. (b) Mirth, G.; Lercher, J. A. *J. Catal*. **1991**, *132*, 244.
(53) Ramanchandran, S.; Lenz, T. G.; Skiff, W. M.; Rappé, A. K. *J. Phys. Chem*. **1996**, *100*, 5898.
(54) Rozanska, X.; Van Santen, R. A.; Hutschka, F.; Hafner, J. *J. Catal*. **2003**, *215*, 20.
(55) Franks, F. *Biophys. Chem*. **2002**, *96*, 117.
(56) Radkiewicz, J. L.; Brooks, C. L., III *J. Am. Chem. Soc*. **2000**, *122*, 225.
(57) Barbosa, L. A. M. M.; Van Santen, R. A. *J. Mol. Catal. A* **2001**, *166*, 101.